Construction and Building Materials 297 (2021) 123785

Contents lists available at ScienceDirect

Construction and Building Materials

journal homepage: www.elsevier.com/locate/conbuildmat

Machine learning model for predicting the crack detection and pattern recognition of geopolymer concrete beams

Aravind N [a], Nagajothi S [b,*], Elavenil S [b]

[a] Department of Civil and Environmental Environment, National University of Science and Technology, Oman
[b] School of Civil Engineering, Vellore Institute of Technology, Chennai Campus, Chennai 127, India

HIGHLIGHTS

- Crack acquisition of experimented geopolymer concrete beams with BFRP & GFRP bars.
- Well-equipped image pre-processing python packages used to collect crack patterns.
- Automated quality check using machine learning python packages.
- Support Vector Machine (SVM) is used to classify the failure patterns.
- SVM compared with other five machine learning classifiers using confusion matrix.

ARTICLE INFO

Article history:
Received 10 January 2021
Received in revised form 19 April 2021
Accepted 27 May 2021

Keywords:
Geopolymer
Pre-processing
Classifiers
Confusion matrix
Machine learning
Python

ABSTRACT

One of the major challenges in the construction industry is the detection of cracks in concrete structures and identification of failure types of these structures that lead to their degradation. Manual quality checks are prone to human error, and require longer response time and specialist experience and knowledge. Therefore, visualizing the cracks and identifying failures in concrete structures using computer techniques is now a preferred option. The present work focuses on identifying the cracks using image processing and failure pattern recognition technique by employing suitable machine learning algorithms, and validating the techniques using Python programming. For this purpose, M30 grade geopolymer and conventional concrete beams were cast using Basalt Fibre Reinforced Polymer/Glass Fibre Reinforced Polymer and Steel bars. The beams were subjected to four point static bending test by varying the shear span to the effective depth ratio. The experimental images were used for image processing and failure pattern recognition in Python language. Employing six machine learning classifiers, the failures in the structures were classified into three classes namely, flexure, shear, and compression. The machine learning classifiers were also adopted to determine the confusion matrix, accuracy, precision, and recall scores. It was found that among the six classifiers used, the support vector classifier gave the best performance with 100% accuracy in identifying the failure patterns.

1. Introduction

Concrete is the main base material for constructing a building with cement being the major ingredient of concrete. Cement manufacturing industries release large amounts of carbon dioxide into the atmosphere. Geopolymer concrete is an innovative and sustainable construction material which consists of three components namely, a source of aluminosilicate materials, fine and coarse aggregate, and an alkali activating solution. Examples of aluminosilicate materials are fly ash, Ground Granulated Blast furnace Slag, slag cement, slag, metakaolin and silica fume. Alkali solution is a mixture of sodium silicate and sodium hydroxide along with water or a mix of potassium silicate and potassium hydroxide along with water. It is used for casting of structural members, pavement construction, brick/ block manufacturing work, etc. When buildings are exposed to aggressive environments in the long term, damages occur which cause degradation of the buildings. The factors involved in degradation of concrete are salt erosion, frost damage, dry shrinkage, earthquakes, and rain water [1]. The degradation levels and carrying capacity of reinforced concrete structures are mainly influenced by the width, length, type, and the number of cracks in the structures [2]. Hence, the

* Corresponding author.
E-mail addresses: aravind@nu.edu.om (N Aravind), naga.jothis2014phd1138@vit.ac.in (S Nagajothi), elavenil.s@vit.ac.in (S Elavenil).

https://doi.org/10.1016/j.conbuildmat.2021.123785
0950-0618/

assessment of cracks in concrete structures is important for inspection, diagnosis, maintenance, and safety life prediction. Crack detection by visual inspection requires more experience, specialist's knowledge, and is tedious, time consuming, and subjective.

Currently, automatic image-based crack detection methods are used along with visual inspection. Many automatic crack detection methods have been proposed during the past few years [3,4]. Due to irregularities in crack size, shape, unevenly elucidated conditions, and blemishes, crack segmentation from the crack images is very difficult. Hence, crack detection is very important, specifically for the variety of cracks in complicated backgrounds. In this study, a crack detection technique is proposed which employs pre-processing of images for extracting crack patterns and classifiers for segregating the class of crack patterns.

The paper is organized as follows: Section 2 presents the relevant review of literature, section 3 describes the materials and methods, section 4 presents the crack analysis, section 5 presents results and discussion, and section 6 concludes the paper.

2. Related work

Several research works have been carried out in the field of crack detection in geopolymer concrete and the techniques used to measure the crack dimensions. Most recently, Amer Hassan et al. have performed an intensive study on geopolymer concrete. Based on their study, it has been concluded that geopolymer concrete is a sustainable construction material thus presenting a new technology that is of significance in the construction industry [5]. Also, as a popular material it has garnered significant attention in the construction industry due to its useful by-product materials, eco-friendly (low 'embodied energy' and low 'embodied CO_2 emission') nature, non-requirement for water curing, economic viability, and conventional concrete-like properties [6,7,8]. Geopolymer concrete has better compressive strength, develops minor cracks, and undergoes only slight damage in the mass at elevated temperatures as compared to Ordinary Portland Cement (OPC) concrete [9,10]. It contains more amorphous phases, less porosity and more pores in the mesopores range than concrete with OPC [11]. The previous research methods for determining the crack width and depth used ultrasound, which is inconvenient to operate since it requires a coupling agent [12]. Fibre optics approaches employed to determine the crack width and location create complexity in measurement [13]. Image-based crack detection methods have been developed in the past 25 years and have been applied to test civil structures such as pavements, bridges, and water retaining structures. Crack detection techniques used in research include image processing methods such as Canny, Fast Fourier Transform, Fast Haar Transform, and Sobel implemented by MATLAB [14], percolation-based approach [4,15,16], stereovision-based approach [2], computational approach [17], image processing methods such as morphological approach and integrated algorithm [18], and Principal Component Analysis (PCA) based algorithm [19]. Another crack detection technique used in concrete bridges is Spatially Tuned Robust Multifeature (STRUM) classifier-based algorithm that uses on-site robotic scanning that delivers 90% accuracy [20].

Wang and Huang [21] used Otsu threshold segmentation algorithm integrated with a modified Sobel operator for crack detection in concrete bridges. Deep fully convolution neural network (FCN) method (using VGG16) was used by Dung and An [22] for detecting the cracks in concrete. Fujita et al. [23] used two pre-processing methods namely, subtraction and line extraction, and a threshold process to separate the cracks from the background in order to assess their accuracy and firmness [24].

Manufactured sand (M−sand) is used currently due to the scarcity of river sand. Steel corrosion is a major problem and requires expensive maintenance, repair, retrofitting, and rehabilitation in reinforced concrete structures. This problem is overcome by using reinforced concrete structures such as Fibre-Reinforced Polymer (FRP) bars that are non-corrosive, light weight, and environment-friendly in nature. This research mainly focuses on studying the experimental shear behaviour of geopolymer concrete beams using BasaltFibre-Reinforced Polymer (BFRP) and Glass Fibre-Reinforced Polymer (GFRP) bars by varying the shear span to the effective depth ratio, crack detection using image processing, and analytical failure pattern recognition using machine learning algorithms in python script.

3. Materials and methods

This section first details the materials and methods used in the study. Next, the experimental setup is described. Finally, the analysis methodology using image processing and machine learning is presented.

3.1. Materials used

The materials used in the study for making geopolymer and conventional concrete are described in the following sub-sections.

3.1.1. Geopolymer and conventional concrete

For making geopolymer concrete, aluminosilicate materials, i.e. fly ash and ground granulated blast furnace slag (GGBS), coarse aggregate, manufactured sand, alkali activator solutions (sodium silicate and sodium hydroxide), and super-plasticizer were used. For making conventional concrete, 53 grade cement, river sand, coarse aggregate and water were used. The chemical composition of the aluminosilicate materials and the physical properties of the concrete materials used for making the geopolymer concrete are presented in Tables 1 and 2.

3.1.2. BFRP, GFRP, steel bars and stirrups

Steel bars of 12 mm, 10 mm and 8 mm diameter were used as reinforcement bars and stirrups, both, in the geopolymer concrete and the conventional concrete. The properties of BFRP, GFRP and steel bars are presented in Table 3.

3.1.3. Mix proportions and mechanical properties

The mix proportion for M30 grade concrete used in this work was chosen from the previous work [25] as per IS 10262 [26]. The volume of binder, fine aggregate, coarse aggregate and liquid used were 380 kg/m^3, 660 kg/m^3, 1189 kg/m^3 and 171 kg/m^3, respectively. In order to produce M30 grade geopolymer concrete, FA and GGBS were taken in the ratio of 80:20. The ratio of liquid to binder was chosen as 0.45. In geopolymer concrete, river sand was fully replaced by M−sand and one percent of naphthalene based

Table 1
Chemical composition of fly ash and GGBS.

Materials	SiO_2	CaO	MgO	Al_2O_3	Fe_2O_3	K_2O	SO_4	Na_2O	LOI
Fly ash (%)	63.32	2.49	0.29	26.76	5.55	0.0002	0.36	0.0004	0.97
GGBS (%)	35.05	34.64	6.34	12.5	0.3	0.6	0.38	0.9	0.26

Table 2
Physical properties of the concrete materials.

Description	Fly Ash	GGBS	Cement	River Sand	M−Sand	Coarse Aggregate
Specific gravity	2.13	2.85	3.13	2.66	2.72	2.73
Fineness modulus	–	–	–	3.04	2.90	–
Water absorption (%)	–	–	–	1.33	1.52	0.64

Table 3
Properties of FRP bars and Steel bars.

Properties	BFRP	GFRP	Steel
Elastic Modulus (GPa)	94	54	200
Tensile Strength (MPa)	513	515	495
Poisson's ratio	0.23	0.24	0.27

super plasticizer was used to achieve the workability of the geopolymer concrete. Geopolymer concrete is mainly made using class F fly ash obtained from North Chennai Thermal power plant station, Chennai. Commercially available GGBS was used as part replacement material for fly ash in this study. The mixture of sodium silicate and sodium hydroxide solution was used as Alkali Activated Solution (AAS). The 8M NaOH flakes were mixed with distilled water a day before its use, to lower down the ambient temperature and then was mixed with Na_2SiO_3 solution to produce alkaline activator solution to accelerate the reactivity of the solution. The sodium silicate solution with sodium hydroxide ratio by mass of 2.5 was used. In the mixing process, fine and coarse aggregates were first mixed in Saturated Surface Dry (SSD) condition in a mixer machine. Then, the binder contents were mixed with the aggregates. The mixing was continued for about 3 min. The already prepared AAS was poured in the mixer machine and the mixing was continued for about 4 min. Finally, the super plasticizer was added to the mixtures to get the required workability until the concrete appeared homogenous and had the desired consistency [27].

Table 4
Mechanical properties of geopolymer and conventional concretes.

Mechanical properties	Geopolymer concrete	Conventional concrete
Compressive strength (MPa)	40.35	38.95
Split tensile strength (MPa)	3.32	3.17
Flexural strength (MPa)	4.69	4.46
Modulus of elasticity (GPa)	19.10	22.19

The mechanical properties of the geopolymer and conventional concretes are tabulated in Table 4 and were validated using the Levenberg–Marquardt training algorithm using MATLAB software [28].

3.2. Methods

3.2.1. Beam details and preparation

Nine concrete beams having width, depth, and length of 100 mm, 160 mm, and 1700 mm, respectively, were cast under four point static bending test with an effective span of 1500 mm. The beam specimen details are illustrated in Fig. 1. Three beams each were cast in BFRP and GFRP bars in geopolymer concrete, and steel bars in conventional concrete. Two 12 mm diameter bars at the bottom and two 10 mm diameter bars at the top, with 8 mm diameter bars as stirrups were used in all the nine beams. The BFRP and GFRP stirrups were prepared by connecting the vertical and horizontal bars (8 mm diameter) using Anabond resin and the joint was connected with FRP mats using epoxy resin. The beams were placed and loaded by varying the ratio of the shear span 'a' to the effective depth 'd' from 3.6 to 4.3. The beams were denoted as follows: BRGC-3.6, BRGC-3.9, BRGC-4.3 for the BFRP bars, GRGC-3.6, GRGC-3.9, GRGC-4.3 for the GFRP bars, and SRCC-3.6, SRCC-3.9, SRCC-4.3 for the steel bars.

After mixing the aggregates in saturated surface dry condition followed by the addition of binders, alkali activated solution, and super plasticizer to the mixer machine, the mix was poured in three layers, and vibrated in beam moulds. The specimens were demoulded after 24 h and kept under ambient curing for geopolymer concrete and under water curing for conventional concrete for 28 days.

3.2.2. Test setup and instrumentation

The details of the loading arrangements with varying ratios of shear span to effective depth are shown in Fig. 2. Details of the test setup and instrumentation are shown in Fig. 3.

Nine beams were tested under four point static bending test by varying the 'a/d' ratio as 3.6, 3.9 and 4.3. The load was applied on

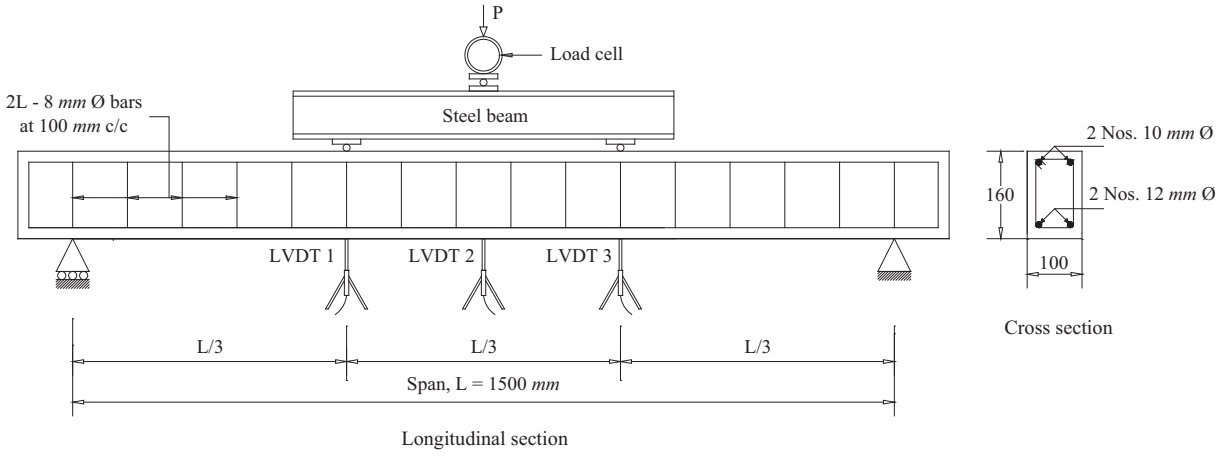

Fig. 1. Reinforcement and Load setup details.

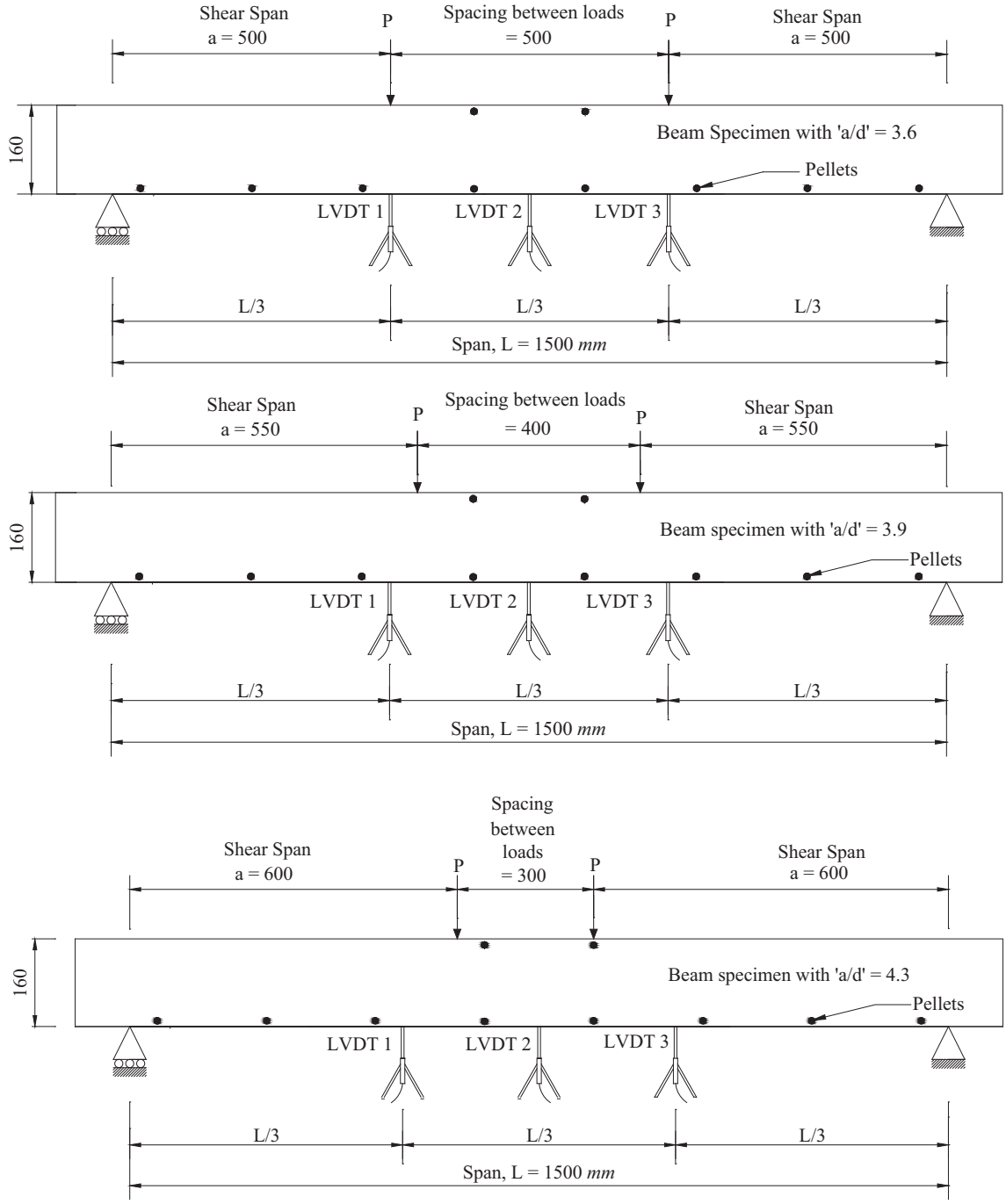

Fig. 2. Details of loading arrangements with 'a/d' ratio of 3.6, 3.9, and 4.3.

the specimens and the cracks for the corresponding load intervals at the time of testing were marked. The crack pattern until failure was also noted.

4. Crack analysis

From the experimental tests [29], the failure mode and crack pattern for all the nine beams subjected to static load by varying the shear span to the effective depth ratio were observed and are shown in Fig. 4.

From Fig. 4 it was observed that when the ratio of the shear span to the effective depth in SRCC was increased, new cracks developed in the outer region of the Constant Bending Moment (CBM) zone (i.e. in the shear zone). But no shear cracks were developed in SRCC-3.6. It was also evident that the mode of failure for SRCC comprises of both flexure and compression with little shear failure as the shear span to effective depth ratio was increased.

The crack patterns were similar in all the beams at initial load intervals. But in BRGC and GRGC beams, it was found that inclined cracks developed from flexural cracks. As compared to BRGC-3.6 and BRGC-4.3, more inclined cracks developed in the shear zone in BRGC-3.9. The same pattern was also observed in GRGC-3.9 when compared to GRGC-3.6 and GRGC-4.3. When the shear span to the effective ratio was 4.3, the beam deflection re-cambered to 20 mm at the ultimate load level after releasing the load for both

Fig. 3. Details of test setup and Instrumentation.

the beams. But for BRGC-3.6, BRGC-3.9, GRGC-3.6, and GRGC-3.9, sudden failure was observed after attaining 95% of the ultimate load level. Thus it can be concluded that sudden shear and flexure failure at premature has occurred. The sudden shear failure observed in GRGC and BRGC beams can be attributed to the insufficient shear reinforcement. The modes of failure and shear strength at ultimate load levels for the steel and geopolymer beams are shown in Table 5.

Table 5 indicates that the ultimate load-carrying capacity and the shear capacity at ultimate load level in the steel and FRP rods decreased as the ratio of the shear span to the effective depth increased. Further, in both the FRP rods, the failure pattern changed from shear to flexure on increasing the 'a/d' ratio from 3.6 to 4.3 while no such change was seen in SRCC.

From the Table 6, it was observed that the number of cracks for steel increased as the ratio of the shear span to the effective depth increased to 3.9, and then decreased with further increase in the 'a/d' ratio to 4.3. The same trend was observed for both the FRP bars. In the case of steel and glass rods, the crack propagation decreased with increase in the shear span to the effective depth ratio while for the basalt reinforced geopolymer concrete beams, the crack propagation reached a high value with increase in this ratio. The spacing of crack decreased when the numbers of cracks and loads increased. The spacing of cracks was constant during the loading and unloading of the ultimate load level for SRCC-4.3 and GRGC-4.3. From table 6, it was observed that the crack spacing decreased suddenly when the load level for SRCC-3.9 increased. When the

(a). Crack pattern and failure mode of Steel reinforced conventional concrete.

(b). Crack pattern and failure mode of Basalt reinforced geopolymer concrete.

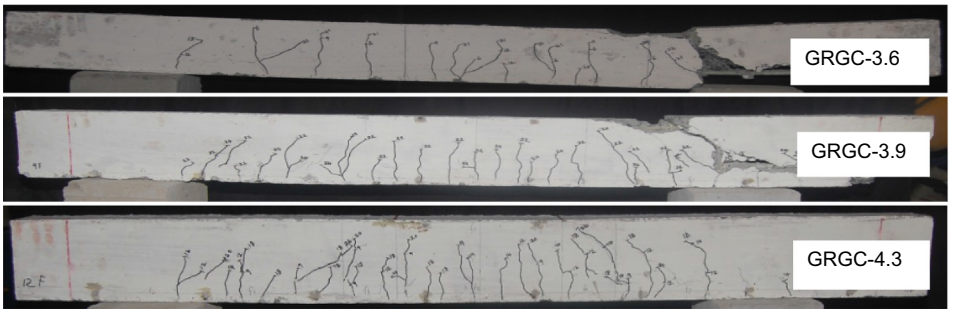

(c). Crack pattern and failure mode of Glass reinforced geopolymer concrete.

Fig. 4. (a). Crack pattern and failure mode of Steel reinforced conventional concrete. **(b).** Crack pattern and failure mode of Basalt reinforced geopolymer concrete. **(c).** Crack pattern and failure mode of Glass reinforced geopolymer concrete.

Table 5
Modes of failure and shear strength at ultimate load levels.

Sl.No	Specimen id	Ultimate Load (kN)	Shear Strength at Ultimate load (MPa)	Failure mode
1	SRCC-3.6	49.80	3.56	Flexure & compression
2	SRCC-3.9	47.95	3.43	Flexure & compression
3	SRCC-4.3	40.20	2.87	Flexure & compression
4	BRGC-3.6	33.45	2.39	Shear compression
5	BRGC-3.9	32.55	2.33	Shear compression
6	BRGC-4.3	32.05	2.29	Flexure
7	GRGC-3.6	32.40	2.31	Shear compression
8	GRGC-3.9	26.65	1.90	Shear compression
9	GRGC-4.3	26.20	1.87	Flexure

Table 6
Behaviour of cracks under static load with varying 'a/d' ratio.

Specimen Id	Total Number of Cracks –First	Total Number of Cracks –Ultimate	Crack Propagation – First	Crack Propagation – Ultimate	Crack spacing – First (CBZ)	Crack spacing – Ultimate (CBZ)	Crack Width –First	Crack Width – Ultimate
	(Nos.)	(Nos.)	(mm)	(mm)	(mm)	(mm)	(mm)	(mm)
SRCC-3.6	5	15	48	116	115	71	0.093	0.4
SRCC-3.9	3	17	70	122	296	126	Nil	0.86
SRCC-4.3	3	11	71	101	97	97	0.355	1.32
BRGC-3.6	9	16	105	130	128	89	0.195	0.56
BRGC-3.9	4	18	85	159	164	75	Nil	1.21
BRGC-4.3	5	16	90	141	123	45	0.064	2.12
GRGC-3.6	6	13	135	153	197	73	0.235	0.78
GRGC-3.9	9	22	95	120	105	57	0.418	1.3
GRGC-4.3	3	11	70	117	135	135	Nil	3.8

ratio of the shear span to the effective depth was increased, the average crack width also increased.

The architecture for crack detection and pattern recognition based on image processing and machine learning algorithm in python script is depicted in Fig. 5.

Machine Learning method is broadly classified into supervised and unsupervised learning. Supervised learning includes Logistic Regression, Naïve Bayes, Stochastic Gradient Descent, K-Nearest Neighbors, Decision Tree, Random Forest, Support Vector Classifier and Deep Learning Neural Network while unsupervised learning comprises of K-Means Clustering, Gaussian Mixture Model and Spectral Clustering. Adaboost is used to combine multiple classifiers. In the present work Stochastic Gradient Descent, K-Nearest Neighbors, Decision Tree and Support Vector Classifier were selected from the supervised learning and Gaussian Mixture Model was chosen from the unsupervised learning. Adaboost was used to combine multiple classifiers. The reason for selecting four machine learning algorithms from the supervised learning is that the training set of data contains observations whose category membership is known. Based on the experimental results, most of the data are known and few data are unknown. Hence, only one machine learning was considered from the unsupervised learning. The above mentioned machine learning applications were used to study various patterns and determine the accuracy of crack detection and pattern recognition.

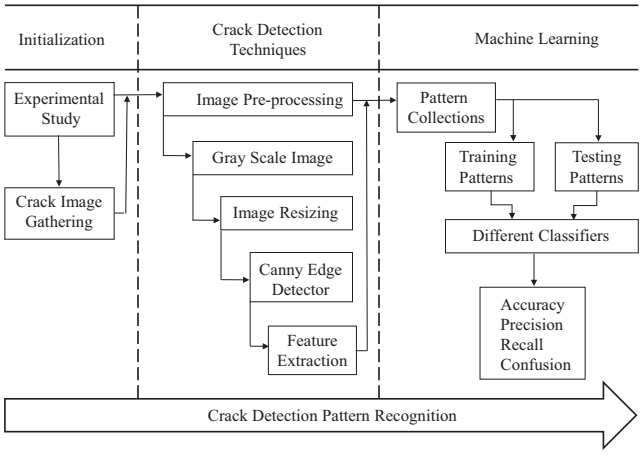

Fig. 5. Architecture for crack detection and pattern recognition.

4.1. Crack image gathering

The images from the structure were captured using a camera and were then subjected to the image pre-processing process and further analysis.

4.2. Image Pre-processing

Image pre-processing comprises of gray scale image conversion, image resizing, canny edge detection, and feature extraction.

4.2.1. Gray scale image conversion

A colour image contains lots of data, most of which are not required for crack detection. Colour images contain RGB (Red, Green, and Blue) colours with different intensity labels, which increase the image size as well as consume more time for processing. Hence conversion of the colour image to gray scale image is necessary to select relevant information, discard unnecessary information and reduce the processing time. In this work, grayscale image conversion was carried out on the input image to convert it from colour to a grayscale image using python package 'skimage.color'. The obtained grayscale image contained a range of black to white shades. Fig. 6(a) depicts the original colour image of the crack with its intensity and Fig. 6(b) depicts the corresponding gray scale image with its intensity. The grayscale image thus obtained was used for image resizing.

4.2.2. Image resizing

The grayscale image was resized to the standard size using python package 'skimage.transform' to avoid unnecessary content in the image and make it ready to identify the cracks. The gray

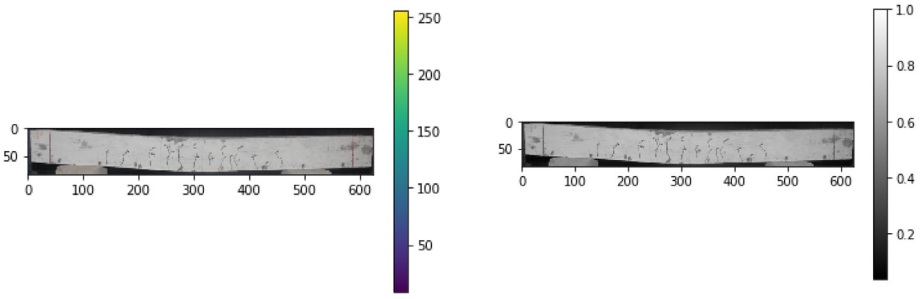

(a) Original colour image and its intensity **(b)**Gray scale image and its intensity.

Fig. 6. Image and intensity details.

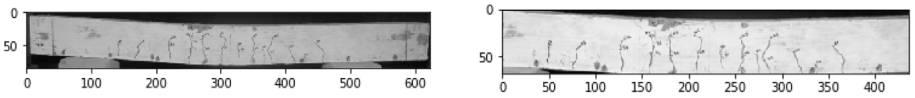

(a) Gray scale image **(b)**Resized gray scale image

Fig. 7. Image scale details.

scale image and the resized gray scale image are shown in Fig. 7(a) and (b). This resized gray scale image was used for further processing.

4.2.3. Canny edge detector

Canny Edge detector is very popular method to separate the background information from the images and to identify the edges as cracks. Canny Edge detector method was implemented using python package 'skimage.feature'.

4.2.4. Work flow of canny edge detector

The Canny edge detector uses the following steps:

i. The image was smoothened using Gaussian filter to eliminate noise.
ii. The intensity gradients of the image were determined.
iii. The false positives in edge detection were eliminated by carrying out Non-maximum suppressing.
iv. The potential boundaries were determined by employing double threshold.
v. Edge tracking was carried out using hysteresis in which edge detection was done by eliminating all weak edges and unconnected to strong edges.

Fig. 8(a) shows the resized gray scale image before applying the canny edge detector function. Fig. 8(b) shows the noise reduced using canny edge detector function with σ = 0.6 and Fig. 8(c) shows the noise further reduced using canny edge detector function with σ = 1.6. It is clear that the noise is reduced fully when the canny edge detector function with parameter σ = 1.6 was applied. Hence, σ plays a key role in the noise reduction in images while using canny edge detector.

4.2.5. Percentile method

Percentile method was used to eliminate outliers in the images. It was implemented using python package 'numpy'. In the present work, the height and width percentile were considered to detect the right crack pattern collection from the image. The resulting patterns are called feature extractions and are shown in Fig. 9.

4.3. Machine learning

Machine learning consists of pattern collection and training, and testing and classification. In this work the machine learning methods were implemented using python package 'sklearn'.

4.3.1. Pattern collection and training

In this stage, the patterns were collected by employing pre-processing techniques and the collected patterns were used to train the classifiers and evaluate the models. The failure patterns of few images is shown in Fig. 10.

4.3.2. Training and testing patterns using different classifiers

To train the patterns and predict the failure pattern in the images, Support vector machine (SVM), Decision tree classifier, Gaussian NB classifier, SGD classifier, K- neighbor classifier and Adaboost classifiers were used. Three classes of pattern failures were considered: flexure, shear, and compression failure, which were treated as target values and subjected to processing by each machine learning classifier.

Of the pattern images, 50% were trained and the remaining 50% were tested. In addition, the performance of each classifier was evaluated using confusion matrix and accuracy score. The evaluation results showed that SVM exhibited the highest accuracy when compared to other classifiers.

4.3.3. Support vector Machine

SVM is a machine learning algorithm used for classifying the different types of cracks and training the machine to identify the correct type of crack pattern failure.

Input parameters used for SVM are as follows:

i. Kernel: Linear
ii. Gamma: 0.0001
iii. Test size: 0.4 (40%)

In general, though SVM is considered as a classification method, it can also be used for regression and classification problems. SVM offers the advantage of simplicity in handling multiple categorical and continuous variables. In SVM, a hyperplane is constructed in

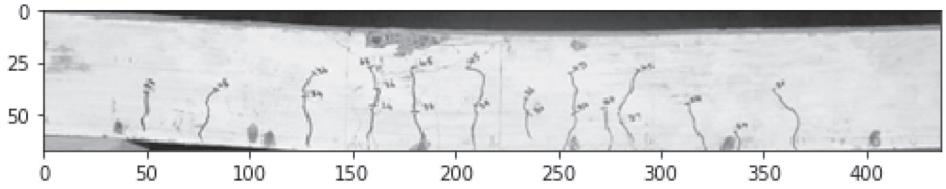

(a). Resized gray scale image before applying canny edge detector function.

(b). Noise reduced using σ =0.6 in canny edge detector function.

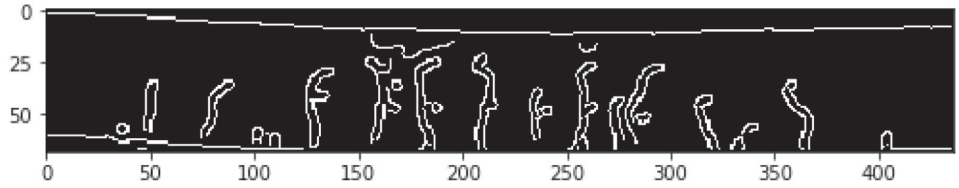

(c). Noise reduced using σ=1.6 in canny edge detector function.

Fig. 8. (a). Resized gray scale image before applying canny edge detector function. **(b).** Noise reduced using σ = 0.6 in canny edge detector function. **(c).** Noise reduced using σ = 1.6 in canny edge detector function.

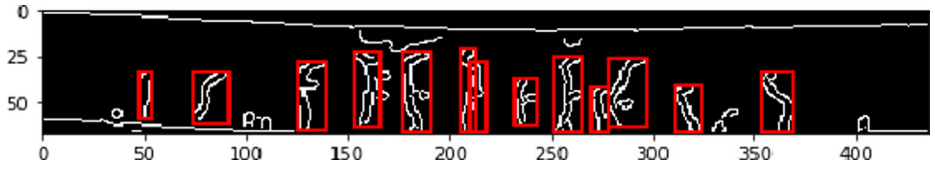

Fig. 9. Feature Extraction of images.

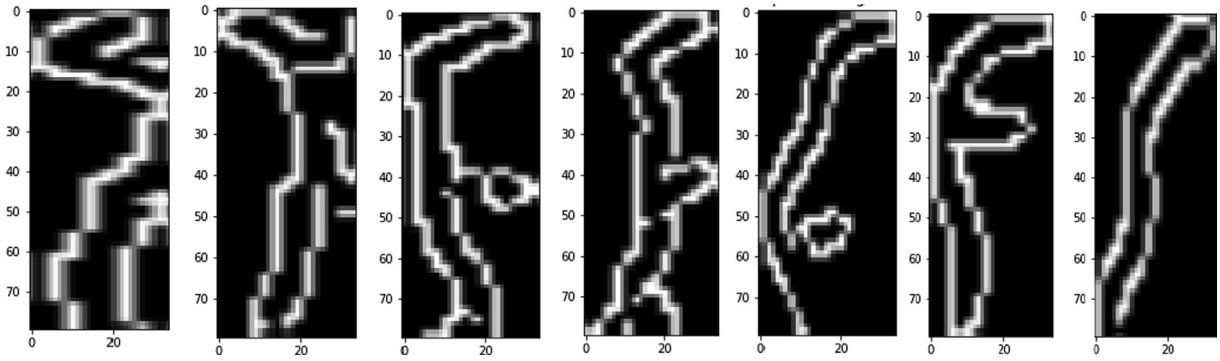

Fig. 10. Failure pattern of images.

multidimensional space for separating various classes. An optimal hyperplane is generated iteratively and is utilized for minimizing the errors. A Maximum Marginal Hyperplane (MMH) is located to perform the division of the dataset as classes in the best manner. Fig. 11 is a representation of SVM showing the support vectors, margins, and hyperplanes.

Support vectors are the data points that are closest to the hyperplane. These points define the separating line effectively by calculating the margins and are more relevant to the construction of the classifier. Hyperplane is a decision plane which separates a set of objects having different class memberships. Margin is the gap between the two lines on the closest class points, which is cal-

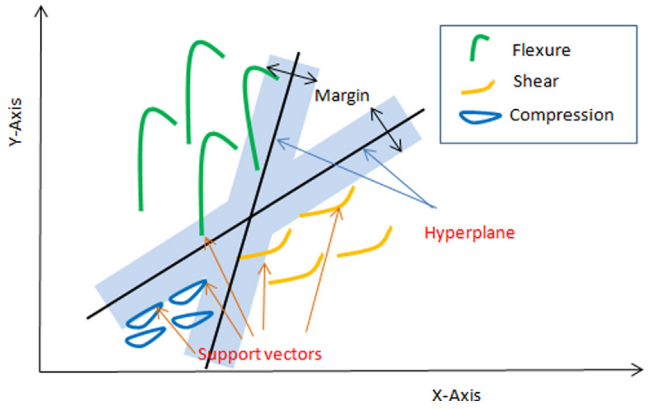

Fig. 11. Representation of SVM.

culated as the perpendicular distance from the line to the support vectors or the closest points. If the margin between the classes is larger it is considered good while a smaller margin is considered bad.

4.3.4. SVM workflow

The main objective is to segregate the given dataset in the best possible way. The distance between the nearest points is known as the margin. The objective is to select a hyperplane with the maximum possible margin between the support vectors in the given dataset. Fig. 12 explains the work flow of SVM when it searches for the MMH.

It is seen in Fig. 12 that the generated hyperplanes segregate the classes in the best possible way. Four hyperplanes are seen: black, blue, orange and purple. The blue and orange hyperplanes have higher classification error while the black and purple hyperplanes separate the three classes correctly.

5. Results and discussions

5.1. Failure pattern identification

The beam images were taken from the experimentally tested beams for training and testing of the models. A total of 232 patterns were taken for evaluating the model. Of the 232 patterns, 139 patterns were used for training, and the remaining 93 patterns were utilized for testing (Fig. 13).

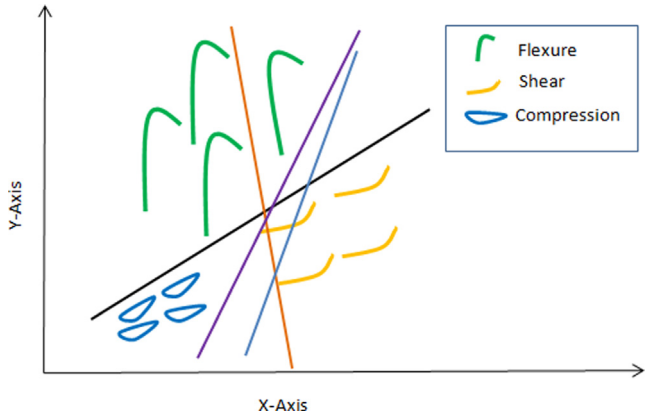

Fig. 12. Work flow of SVM.

5.2. Evaluating the model

The accuracy of the classifier or model for predicting the type of failures in the crack was estimated. Accuracy was computed by comparing the actual test set values and predicted values using confusion matrix. The accuracies of the different classifiers for flexure, shear and compression pattern are shown in Table 7.

From Table 7, it was observed that the accuracy, precision, and recall values for all the pattern classes are the best for the support vector classifier when compared with the other classifiers. The confusion matrix is a Table which describes the performance of the classifiers using the test data. The confusion matrix for SVM, Decision tree classifier, Gaussian NB classifier, SGD classifier, K-neighbor classifier and Adaboost classifier is depicted in Fig. 14 as normalized values.

Fig. 14 indicates that the confusion matrix for SVM shows very good performance in all the three classes (compression, flexure, and shear). The performance and accuracy of SVM is the best among all the classifiers.

Decision tree classifier can cause a big variation and instability even with small data variations. Calculations in Decision tree classifier get more complex than in other algorithms with the model training time also being longer. The problem with Gaussian NB classifier is in its implicit assumption that all attributes are mutually independent, which is impossible in real life. Owing to frequent updates, steps taken by SGD classifier to reach the minima are most noisy, often leading to falling gradient towards other directions. The noisy steps make the loss function minima convergence longer. The K- neighbor classifier, on the other hand, does not perform well when datasets are large. It also performs poorly with high dimensions, since it is difficult for the classifier to calculate each dimension's distance and hence works poorly with more noise in the dataset. Adaboost too is sensitive to outliers and noise. If the data is imbalanced, the classifying accuracy is affected.

There have been a few studies on crack analysis using SVM. Prasanna et al. [30] proposed a crack detection technique for concrete bridges. They compared the results of SVM, Random Forest, and Adaboost classifiers and found that Adaboost was the most accurate with an accuracy of 90.8%. However, the other two classifiers also performed well. Li et al. [31] studied cracks in bridges using greedy-SVM for feature selection. They obtained a crack analysis accuracy of 93.6%. Kim et al. [32] proposed a speeded-up robust features model for crack detection in concrete. Classification was done by linear SVM. The model outperformed the other models by yielding an accuracy of 98%. Another model was proposed by Liang et al. [33] for concrete crack analysis that used the OTSU algorithm for segmentation and SVM for classification. The model gave an accuracy of 100% in the test set identification. Zhang et al. [34] in their proposal, modeled an automatic crack detection and classification method for subway tunnel safety monitoring. For feature extraction, a distance histogram-based shape descriptor was used while different classifiers were used for classification. The Extreme Learning Machine classifier worked best with an accuracy of 91.6%, while the SVM also performed similarly well (accuracy 91.3%). Xie et al. [35] studied voids within RCC structures that impact the structure's safety using GPR images. Their automated model was based on a novel SVM algorithm. Accuracy of up to 97.7% for void identification was obtained using this model.

From the present study it is evident that the SVM is generally more accurate when compared to other classifiers. SVM can easily manage complex non-linear data points and over-fitting issues are lesser than that in other classifiers. SVM also shows better performance in high dimension spaces and in situations where the number of dimensions exceeds the number of samples.

Experimental analysis and machine learning model for predicting the crack detection and pattern recognition for the reinforced

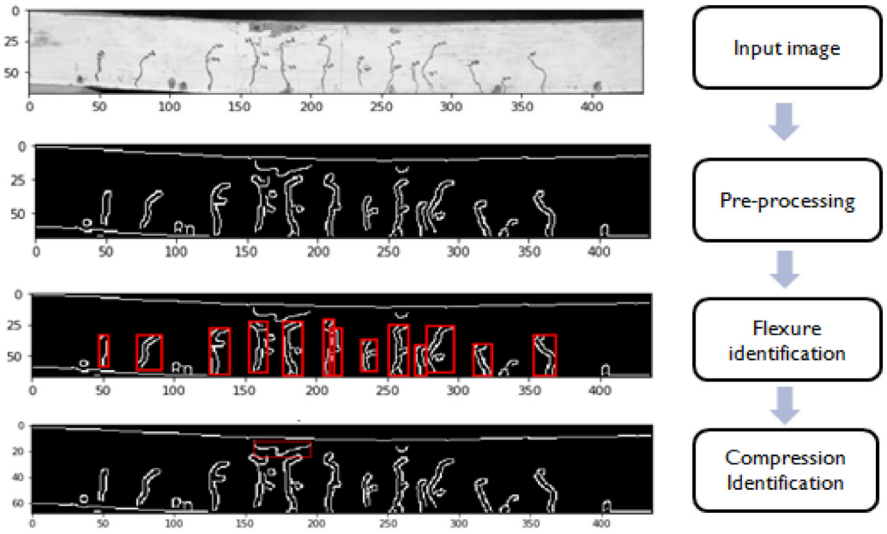

(a). Patterns for model evaluation of beam with Steel bars (SRCC-3.9).

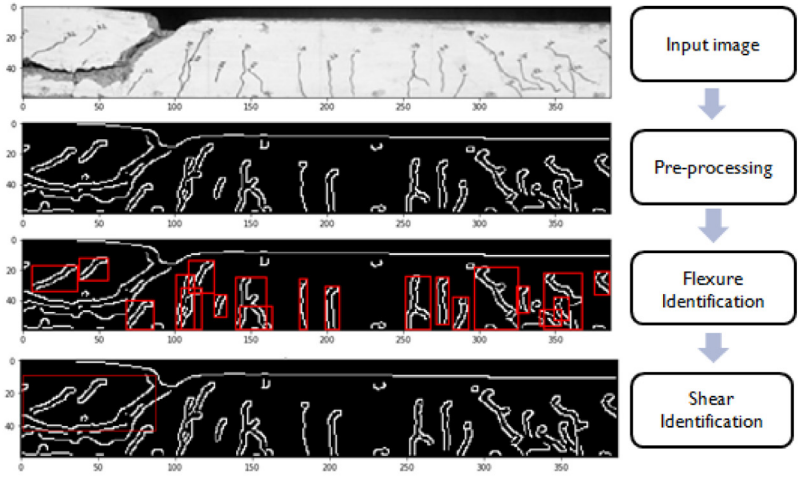

(b). Patterns for model evaluation of beam with Basalt bars (BRGC-3.9).

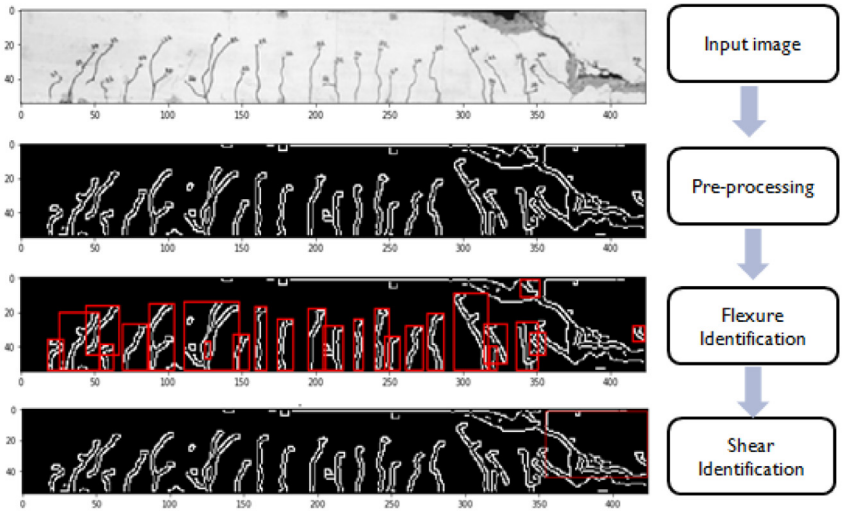

(c). Patterns for model evaluation of beam with Glass bars (GRGC-3.9).

Fig. 13. (a). Patterns for model evaluation of beam with Steel bars (SRCC-3.9). **(b).** Patterns for model evaluation of beam with Basalt bars (BRGC-3.9). **(c).** Patterns for model evaluation of beam with Glass bars (GRGC-3.9).

Table 7
The accuracies of different classifiers for flexure, shear, and compression pattern.

Classifiers/Patterns	Flexure pattern			Shear pattern			Compression pattern		
	Accuracy (%)	Precision	Recall	Accuracy (%)	Precision	Recall	Accuracy (%)	Precision	Recall
Support vector	100	1.00	1.00	100	1.00	1.00	100	1.00	1.00
Decision tree	97	1.00	0.94	97	0.93	1.00	88	0.79	1.00
Gaussian NB	99	0.99	1.00	90	1.00	0.82	100	1.00	1.00
SGD	98	1.00	0.96	90	0.82	1.00	100	1.00	1.00
K- neighbor	98	1.00	0.96	100	1.00	1.00	88	0.79	1.00
Adaboost	99	0.99	1.00	96	0.93	1.00	100	1.00	1.00

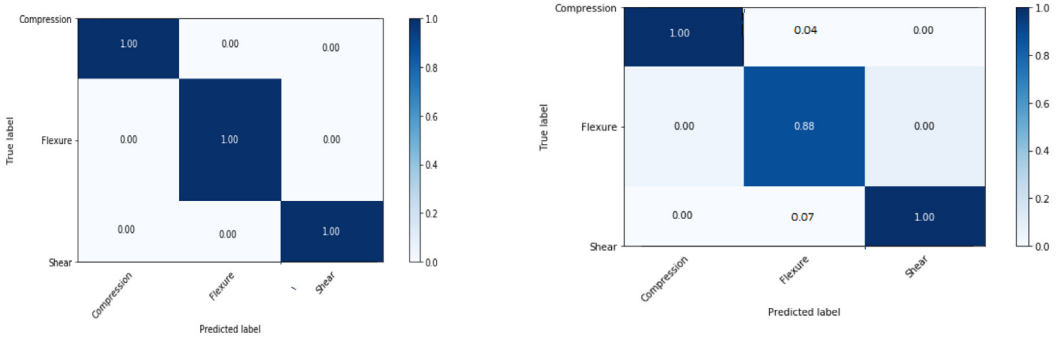

(a) SVM

(b) Decision tree classifier

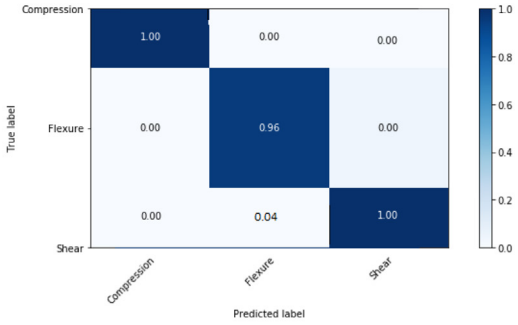

(c) Gaussian NB classifier

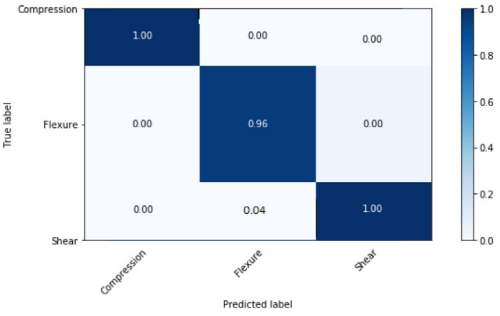

(d) SGD classifier

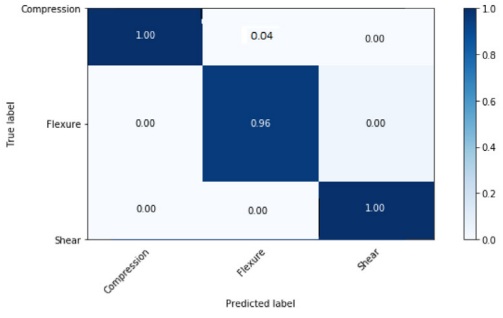

(e) K- neighbor classifier

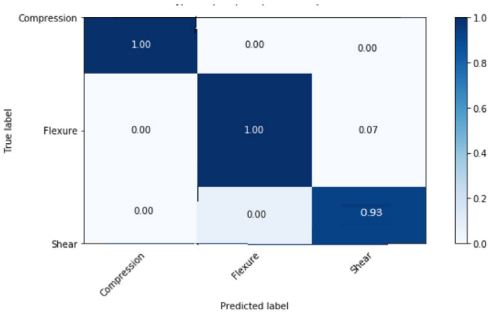

(f) Adaboost classifier

Fig. 14. Confusion matrix for different classifiers.

concrete without cement and steel reinforcement is the novelty of the present research work. The cement concrete and steel reinforcement were replaced by geopolymer concrete and BFRP/ GFRP bars, respectively and were used as longitudinal reinforcements for casting and testing. For reinforced concrete, lots of codes of practice/ standards are available for the shear, flexure, deflection and crack width analysis. On the other hand, no code has been published to date for the geopolymer concrete reinforced with BFRP/ GFRP bars. Machine Learning technique is the only option to predict the crack detection for the geopolymer concrete and BFRP/ GFRP bars combination. Coefficients of thermal expansion for conventional cement concrete and steel bars are almost the same. In contrast, the coefficient of thermal expansion of fly ash geopolymer concrete is in the range of 5×10^{-6}/°C to 13×10^{-6}/°C. The specific

properties of geopolymer concrete depend on the source/ raw materials used for the specimen preparation. Pavalan V. and Sivagamasundari R have conducted experimental study to determine the thermal expansion coefficient of various FRP bars. Based on the studies, the coefficient of longitudinal thermal expansion of BFRP and GFRP bars are around 2×10^{-6}/°C and 9×10^{-6}/°C, respectively [36]. Owing to the variation in the coefficient of thermal expansion, machine learning technique was adopted for the crack identification and damage pattern recognition of geopolymer concrete reinforced with BFRP/ GFRP bars.

6. Conclusions

If pre-processing techniques and pattern classifier techniques are robust, then high accuracy can be obtained for pattern recognition very easily. In this research, pre-processing techniques such as Gray-scale image conversion, Image resizing, Canny edge detector and Percentile method were used and validated for the extracted crack patterns.

Different classifiers namely, SVM, Decision tree classifier, Gaussian NB classifier, SGD classifier, K-neighbour classifier, and Adaboost classifier were used to segregate the compression, flexure, and shear classes of patterns from the given crack patterns. Among these classifiers, SVM recorded the best performance and accuracy for prediction of crack failures across all three classes, whereas other classifiers performed well only for one or two classes.

The present research work recommends that the geopolymer reinforced concrete prepared with fly ash, GGBS, manufactured sand and GFRP/ BFRP bars can be used as alternative/ sustainable materials for cement, fine aggregates and steel bars, respectively. Flexural members of concrete structures prepared with GFRP/ BFRP bars and a geopolymer concrete combination is supportive to avoid reinforcement corrosion and reduce air pollution. In the present study, various machine learning methods were adopted to classify several types of cracks in geopolymer concrete beams. The crack analysis proved that staged image processing techniques and machine learning classifiers used in this research work are greatly advantageous in the detection of tensile, shear, and compression cracks in reinforced concrete beams.

CRediT authorship contribution statement

N. Aravind: Validation, Investigation. **S. Nagajothi:** Writing - original draft, Visualization, Methodology, Conceptualization, Investigation, Resources, Validation, Software, Data curation. **S. Elavenil:** Formal analysis, Supervision, Investigation, Validation, Writing-review & editing.

Declaration of Competing Interest

The authors declare that they have no known competing financial interests or personal relationships that could have appeared to influence the work reported in this paper.

Acknowledgements

Authors would like to acknowledge the Management and Dean-School of Civil Engineering, Vellore Institute of Technology, Chennai, India for providing the necessary support to carry out this research.

References

[1] Tomoyuki Yamaguchi, Shingo Nakamura, RyoSaegusa and Shuji Hashimoto, Image-Based Crack Detection for Real Concrete Surfaces, Transactions on Electrical and Electronic Engineering, IEEJ Trans 2008; 3: 128–135, Published online in Wiley Inter Science (www.interscience.wiley.com). DOI:10.1002/tee.20244.
[2] B. Shan, S. Zheng, O.u. Jinping, A stereovision-based crack width detection approach for concrete surface assessment, KSCE J. Civ. Eng. 20 (2) (2016) 803–812.
[3] H. Nakamura, R. Sato. K. Kawamura, A. Miyamoto. Proposal of a crack pattern extraction method from digital images using an interactive genetic algorithm. Japan Society of Civil Engineers, 60 (742) 115–131, September 2003 (in Japanese).
[4] T. Yamaguchi, K. Suzuki, P. Hartono, S. Hashimoto, Percolation approach to image-based crack detection, in: Proceedings of the 7th international conference on Quality Control by Artificial Vision, 2005, pp. 291–296.
[5] Amer Hassan, Mohammed Arif and M. Shariq, Effect of Curing Condition on the Mechanical Properties of Fly Ash based Geopolymer Concrete, SN Applied Sciences, Springer Nature, 1:1694, 2019. https://doi.org/10.1007/s42452-019-1774-8.
[6] Amer Hassan, Mohammed Arif, M. Shariq, Use of geopolymer concrete for a cleaner and sustainable environment - A review of mechanical properties and microstructure, J. Clean. Prod. Elsevier, 223, (2019) 704-728. https://doi.org/10.1016/j.jclepro.2019.03.051.
[7] Amer Hassan, Mohammed Arif, M. Shariq, Mechanical behaviour and microstructural investigation of geopolymer concrete after exposure to elevated temperatures, Arabian J. Sci. Eng., Springer, 45, (2020), 3843–3861. https://doi.org/10.1007/s13369-019-04269-9.
[8] A. Hassan, M. Arif, M. Shariq, A review of properties and behaviour of reinforced geopolymer concrete structural elements - A clean technology option for sustainable development, J. Clean. Prod. 245 (2020), https://doi.org/10.1016/j.jclepro.2019.118762 118762.
[9] A. Hassan, M. Arif, M. Shariq, Age-dependent compressive strength and elastic modulus of fly ash-based geopolymer concrete, structural concrete, J. Fib. (2020), https://doi.org/10.1002/suco.202000372.
[10] A. Hassan, M. Arif, M. Shariq, Structural performance of ambient cured reinforced geopolymer concrete beams with steel fibres, structural concrete, J. Fib. (2020), https://doi.org/10.1002/suco.202000191.
[11] Influence of Microstructure of Geopolymer Concrete on its Mechanical Properties — A Review 35 (2020), https://doi.org/10.1007/978-981-13-7480-7_10.
[12] D. McCann, M. Forde, Review of NDT methods in the assessment of concrete and masonry structures, NDT & E Int. 34 (2) (2001) 71–84, https://doi.org/10.1016/S0963-8695(00)00032-3.
[13] W.T. Zhang, J.Y. Dai, H. Xu, B.C. Sun, Y.L. Du. Distributed fiber optic crack sensor for concrete structures." Proc. of SPIE, Sandiego, USA, 6830 (2007) 68300F, DOI: 10.1117/12.757864.
[14] Ikhlas Abdel-Qader, Osama Abudayyeh, Michael E. Kelly, Analysis of edge detection techniques for crack identification in bridges, J. Comput. Civ. Eng. Am. Soc. Civ. Eng. 17 (3) (2003) 255–263.
[15] T. Yamaguchi, S. Hashimoto, Automated Crack Detection for Concrete Surface Image Using Percolation Model and Edge Information, 1-4244-0136-4/06 (2006) IEEE.
[16] T. Yamaguchi, K. Suzuki, P. Hartono, S. Hashimoto. An efficient crack detection method using percolation-based image processing, Proc. of ICIEA2008, 3 (1875-1880) (2008).
[17] John Canny, A Computational Approach to Edge Detection, IEEE Transactions on Pattern Analysis and Machine Intelligence, PAMI-8 (6) NOVEMBER 1986.
[18] H. Wang Pand Huang, Comparison Analysis on Present Image-based Crack Detection Methods in Concrete Structures, 3rdInternational Congress on Image and Signal Processing, 2010.
[19] I. Abdel-Qader, S. Pashaie-Rad, O. Abudayyeh, S. Yehia, PCA-Based algorithm for unsupervised bridge crack detection, Adv. Eng. Softw. 37 (2006).
[20] Prateek Prasanna, Kristin J. Dana, Nenad Gucunski, Basily B. Basily, Hung M. La, Ronny Salim Lim, Hooman Parvardeh, IEEE Trans. Automat. Sci. Eng. 13 (2) (2016) 591–599.
[21] Yun Wang, Ju Yong Zhang, Jing Xin Liu, Yin Zhang, Zhi Ping Chen, Chun Guang Li, Kai He, Rui Bin Yan, Research on Crack Detection Algorithm of the Concrete Bridge Based on Image Processing, 8thInternational Congress of Information and Communication Technology, ICICT 2019, Procedia Computer Science 154 (2019) 610–616.
[22] Cao Vu Dunga, Le DucAnh, Autonomous concrete crack detection using deep fully convolutional neural network, Automat. Constr. 99 (2019) 52–58.
[23] Yusuke Fujita, Yoshihiro Mitani, Yoshihiko Hamamoto, A Method for Crack Detection on a Concrete Structure, 18thInternational Conference on Pattern Recognition (ICPR'06) 0-7695-2521-0/06, 2006.
[24] S. Nagajothi, S. Elavenil, Parametric studies on the workability and compressive strength properties of geopolymer concrete, J. Mech. Behav. Mater. 20180019 (2018) 1–11.
[25] S. Nagajothi, S. Elavenil, GGBFS & M-Sand impact on workability and strength properties of fly ash based geopolymer concrete, Indian J. Eng. Mater. Sci. 27 (2020) 67–76.
[26] IS 10262, Indian Standard recommended guidelines for concrete mix design. Bureau of Indian Standards, New Delhi 2009.
[27] S. Nagajothi, S. Elavenil, Experimental investigations on compressive, impact and prediction of stress-strain of fly ash-geopolymer and portland cement concrete, J. Polym. Eng. 40 (7) (2020) 583–590.
[28] S. Nagajothi, S. Elavenil, Influence of aluminosilicate for the prediction of mechanical properties of geopolymer concrete – Artificial Neural Network, Silicon 12 (2020) 1011–1021.

[29] S. Nagajothi, S. Elavenil, Shear Prediction of geopolymer concrete beams using Basalt/Glass FRP bars, J. Adv. Concr. Technol. 19 (2021) 216–225.
[30] P. Prasanna, K.J. Dana, N. Gucunski, B.B. Basily, H.M. La, R.S. Lim, H. Parvardeh. Automated crack detection on concrete bridges, IEEE Trans. Automat. Sci. Eng. 13(2) (2014) 591-599.
[31] G. Li, X. Zhao, K. Du, F. Ru, Y. Zhang, Recognition and evaluation of bridge cracks with modified active contour model and greedy search-based support vector machine, Automat. Constr. 78 (2017) 51–61.
[32] H. Kim, E. Ahn, M. Shin, S.H. Sim, Crack and non-crack classification from concrete surface images using machine learning, Struct. Health Monit. 18 (3) (2019) 725–738.
[33] S. Liang, X. Jianchun, Z. Xun, An algorithm for concrete crack extraction and identification based on machine vision, IEEE Access 6 (2018) 28993–29002.
[34] W. Zhang, Z. Zhang, D. Qi, Y. Liu. Automatic crack detection and classification method for subway tunnel safety monitoring. Sensors, 14(10) (2014) 19307-19328.
[35] X. Xie, P. Li, H. Qin, L. Liu, D.C. Nobes, GPR identification of voids inside concrete based on the support vector machine algorithm, J. Geophys. Eng. 10 (3) (2013) 034002.
[36] V. Pavalan, R. Sivagamasundari, Thermal expansion coefficient of basalt fibre reinforced polymer bars, Int. J. Res. Eng. Appl. Manag. 5 (1) (2019) 414–418, https://doi.org/10.18231/2454-9150.2019.0333.